

Article

Modelling of an Atmospheric-Pressure Air Glow Discharge Operating in High-Gas Temperature Regimes: The Role of the Associative Ionization Reactions Involving Excited Atoms

Ezequiel Cejas ¹ , Beatriz Mancinelli ¹ and Leandro Prevosto ^{2,*}

¹ Grupo de Descargas Eléctricas, Departamento Ing. Electromecánica, Facultad Regional Venado Tuerto (UTN), Laprida 651, Venado Tuerto, 2600 Santa Fe, Argentina; cejasezequiel87@gmail.com (E.C.); beatrizmancinelli@frvt.utn.edu.ar (B.M.)

² CONICET, Facultad Regional Venado Tuerto Departamento Ing. Electromecánica, Grupo de Descargas Eléctricas, Universidad Tecnológica Nacional, Laprida 651, Venado Tuerto, 2600 Santa Fe, Argentina

* Correspondence: prevosto@waycom.com.ar

Received: 17 December 2019; Accepted: 21 January 2020; Published: 18 February 2020



Abstract: A model of a stationary glow-type discharge in atmospheric-pressure air operated in high-gas-temperature regimes ($1000\text{ K} < T_g < 6000\text{ K}$), with a focus on the role of associative ionization reactions involving $\text{N}(^2\text{D}, ^2\text{P})$ -excited atoms, is developed. Thermal dissociation of vibrationally excited nitrogen molecules, as well as electronic excitation from all the vibrational levels of the nitrogen molecules, is also accounted for. The calculations show that the near-threshold associative ionization reaction, $\text{N}(^2\text{D}) + \text{O}(^3\text{P}) \rightarrow \text{NO}^+ + \text{e}$, is the major ionization mechanism in air at $2500\text{ K} < T_g < 4500\text{ K}$ while the ionization of NO molecules by electron impact is the dominant mechanism at lower gas temperatures and the high-threshold associative ionization reaction involving ground-state atoms dominates at higher temperatures. The exoergic associative ionization reaction, $\text{N}(^2\text{P}) + \text{O}(^3\text{P}) \rightarrow \text{NO}^+ + \text{e}$, also speeds up the ionization at the highest temperature values. The vibrational excitation of the gas significantly accelerates the production of $\text{N}_2(\text{A}^3\Sigma_u^+)$ molecules, which in turn increases the densities of excited $\text{N}(^2\text{D}, ^2\text{P})$ atoms. Because the electron energy required for the excitation of the $\text{N}_2(\text{A}^3\Sigma_u^+)$ state from $\text{N}_2(\text{X}^1\Sigma_g^+, v)$ molecules (e.g., 6.2 eV for $v = 0$) is considerably lower than the ionization energy (9.27 eV) of the NO molecules, the reduced electric field begins to noticeably fall at $T_g > 2500\text{ K}$. The calculated plasma parameters agree with the available experimental data.

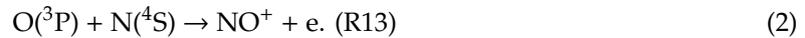
Keywords: glow discharge; air; ionization kinetics

1. Introduction

Several kinetic schemes have been proposed in the literature for modelling atmospheric pressure nonequilibrium air discharges, such as streamers [1,2], low-current arc and glow discharges at rest (or in low gas flows) [3–6], glow discharges in fast gas flows [7–9], and high-current pulsed discharges [10–15]. It is found that the ionization by electron impact of O_2 and N_2 molecules dominates at low-gas temperature (T_g is below the range of 1000–2000 K [10,14,15]), while the electron-impact ionization of NO molecules is written as:



where R refers to the reactions used in the model. This electron-impact ionization is favored by its low ionization energy of 9.27 eV and dominates at high gas temperatures [3,4,14,15]. At $T_g > 4500$ K, the associative ionization in ground-state atomic collisions can be shown as:



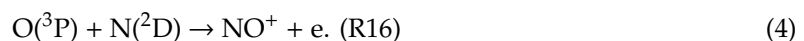
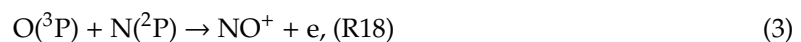
The ionization rate is independent of the reduced electric field, because the densities of both $\text{O}(^3\text{P})$ and $\text{N}(^4\text{S})$ depend only on T_g [3,4,10,13,15], which becomes the dominant ionization mechanism in air. This transition leads to a sharp drop in the reduced electric field [10].

The high efficiency of associative ionization reactions involving nitrogen and oxygen atoms is explained by a decrease in the ionization threshold at the expense of the energy of the resultant chemical bond. For instance, reaction (R13) has an activation barrier of 2.76 eV for ground-state reactants and is therefore assumed to be the dominant ionization mechanism in high-gas-temperature air, where the reduced electric field is low, (i.e., $E/N < 20$ Td, where E is the electric field strength and N is the neutral gas density). As the reduced field increases, both vibrational and electronic excitations come into play. As a result, more efficient channels for associative ionization may appear [16]. However, despite the great interest and importance of ionization processes in hot air discharges, the influence of the electronically excited states of reactants on associative ionization processes is yet unclear, as they are not routinely considered in air kinetic models [1–15]. To answer this question, it is necessary to carry out more comprehensive investigations. This paper is an effort to address this issue.

Recently, a kinetic model [17] that considered associative ionization reactions involving $\text{N}(^2\text{D}, ^2\text{P})$ -excited atoms was presented. The model was applied to the modelling of nonequilibrium air plasmas created by glow discharges in a fast longitudinal air flow. High-speed gas flows were used to provide sufficient cooling of discharges at high pressures. If the gas residence time in the discharge was small as compared with the vibrational-to-translational (V–T) energy relaxation time, gas heating was almost suppressed and the molecular gas was in a strongly nonequilibrium state [8,9]. This state was characterized by a level of vibrational energy that considerably exceeded its equilibrium value. On the other hand, for discharge conditions that the gas residence time in the discharge was larger than the V–T relaxation time (e.g., ambient air discharges), the molecular gas changed to a state close to the thermodynamically equilibrium one with a higher gas temperature, as in an arc discharge. In this work, a kinetic model [17] was used for simulation of stationary glow discharges operated in ambient air at high-gas-temperature regimes ($1000 \text{ K} < T_g < 6000 \text{ K}$) over a wide current density range. The major difference between the kinetic schemes proposed in the literature for modelling atmospheric-pressure air glow discharges [3–9] and the one used in this work is that the present model takes into account ionization processes involving excited-state atomic collisions. The results indicated a strong impact of these reactions under the conditions considered. The calculated plasma parameters agreed with the available experimental data.

2. Modeling of an Atmospheric-Pressure Air Glow Discharge Operated in High-Gas-Temperature Regimes

A nitrogen–oxygen (N_2 –20% O_2) mixture was considered. A kinetic model included processes involving positive ions (i.e., NO^+ , N_2^+ , O_2^+ , and O^+) and negative ions (O^- , O_2^- , and O_3^-), neutral species (i.e., $\text{N}_2(\text{X}^1\Sigma_g^+, \nu)$, $\text{N}_2(\text{A}^3\Sigma_u^+)$, $\text{N}_2(\text{B}^3\Pi_g)$, $\text{N}_2(\text{a}^1\Sigma_u^-)$, $\text{N}_2(\text{C}^3\Pi_u)$, $\text{N}(^2\text{D})$, $\text{N}(^4\text{S})$, $\text{N}(^2\text{P})$, $\text{O}(^3\text{P})$, $\text{O}(^1\text{D})$, $\text{O}(^1\text{S})$, O_2 , and NO), and electrons (e). As a distinctive feature, the model incorporated an exoergic associative ionization reaction with the participation of $\text{N}(^2\text{P})$ atoms [18,19] and a near-threshold reaction with the participation of $\text{N}(^2\text{D})$ atoms with a low activation barrier of 0.38 eV [20,21], which can be described as:



Note that associative ionization reactions with the participation of $N(^2D, ^2P)$ metastable atoms were also included in the kinetic model presented in [22] for modelling nonequilibrium discharges in oxygen–nitrogen mixtures. However the present conditions (i.e., high gas temperature ($1000\text{ K} < T_g < 6000\text{ K}$) and vibrationally excited air discharges) are quite different to those conditions (i.e., low gas temperature ($200\text{ K} < T_g < 500\text{ K}$) and vibrationally unexcited gas) considered in [22]. Since a non-negligible amount of electron energy lost in vibrational excitation can be recovered by electrons in superelastic collisions, the present model also included the effects of these collisions on the enhancing of the tail of the electron energy distribution function which can lead to an increase of some electron-impact rate coefficients by several orders of magnitude [23]. Furthermore, the thermal dissociation of vibrationally excited nitrogen molecules, as well as the electronic excitation from all the vibrational levels of $N_2(X^1\Sigma_g^+, v)$ molecules, was also considered. The main reactions are presented in Appendix A (Table A1).

It should be noted that the proposed reaction kinetic scheme did not include three-body reactions for the generation of N_4^+ and O_4^+ . These cluster ions play only a dominant role in atmospheric-pressure air discharges at low gas temperature ($T_g < 900\text{ K}$). Gas heating beyond 900 K results in the total decomposition of such cluster ions through the processes, which are reverse to three-body reactions for the generation of N_4^+ and O_4^+ , because of the low dissociation energy of these ions [13].

The balance equations for the species $N_2(A^3\Sigma_u^+)$, $N_2(a'^1\Sigma_u^-)$, NO , $N(^4S)$, $N(^2D)$, $N(^2P)$, $O(^3P)$, $O(^1D)$, $O(^1S)$, N_2^+ , O_2^+ , O^+ , O^- , O_2^- , O_3^- , and electrons were solved in a local (volume-averaged) approximation. In stationary high-pressure plasmas, this approximation is usually justified at a long-time scale for diffusive losses, rather than at a relatively short-time scale, to achieve local equilibrium [24]. The rate for the production of the $N_2(A^3\Sigma_u^+)$ state by cascading was assumed to be equal to the sum of the rates for the production by the electron impact of the $N_2(B^3\Pi_g)$ and $N_2(C^3\Pi_u)$ states [3,25]. The plasma quasi-neutrality equation was used to identify the density of NO^+ —the dominating ion under the conditions considered. The densities of $N_2(X^1\Sigma_g^+, v)$ and O_2 were given by the condition of conservation of N and O nuclei. A pressure ($p = 1\text{ atm}$) was assumed in the calculations. The model was complemented with the balance equation depicting the mean vibrational energy of nitrogen molecules as well as the mean kinetic energy of the gas. The time of V–T relaxation of $N_2(X^1\Sigma_g^+, v)$ on $O(^3P)$ was taken from [26–28]. The “fast” gas heating in chemical reactions [29] was also taken into account for reactions, where energy release was considered accompanied by the exothermic energy value on the right side of the reactions in Table A1 (Appendix A). More details in the equations of the model and the treatment of the source terms can be found in [17]. The radial heat loss by thermal conduction—the dominant discharge cooling mechanism under the present conditions [5]—was calculated, considering a parabolic radial profile for the gas temperature in a discharge column with a characteristic radius R of approximately 1 mm (e.g., [30]). The translational thermal conductivity of heavy particles was taken from [31].

3. Results and Discussion

Low-current discharges in atmospheric-pressure air have been studied in a number of experiments (see recent reviews [32–34] and references therein). In most of the experiments, for which current density values j are available [3,35–45], the current discharge radius was inferred by the emission spectroscopy of the $N_2\text{ C}$ state. However, the emission discharge and the current discharge radii may be not equal, and both their radii (and their ratios) depend on experimental conditions [5,46]. As a result, variation of cathode materials (e.g., glow discharges with liquid [35,40,41], plasma [36,37], or metal [3,38,39,42–45] cathodes), stabilization modes (with or without tubes and flows as well as swirl versus axial flows [38]), or the electrode gaps and of discharge currents causes a large scatter of discharge parameter data in terms of the current density. In any case, since the C state of N_2 is produced by electron-impact excitation, the available current density values are representative of regions with high electron number density. As a consequence, the model output gives estimations of discharge variables evaluated at the center of the discharge column.

Figure 1 shows the electron temperature, the gas temperature, and the vibrational temperature of the $N_2(X^1\Sigma_g^+, v)$ molecules versus the discharge current density for radii R of 1 and 2 mm. Experimental data are also shown in Figure 1. The difference between the vibrational and gas temperatures increased substantially with a decrease in j (or in R), due to the strong dependence of the V–T energy relaxation rate on T_g . Considering the uncertainty in the experimentally inferred j values, the results of the calculations for $R = 1.0$ mm were in fairly good agreement with experimental data [39,41,43–45]. On the other hand, the calculated and measured distributions did not coincide for the larger R value. The electron temperature gently decreased with values around 7000–9000 K, as the discharge current density increased, which is typical of glow-type discharges in molecular gases (e.g., [3,4]).

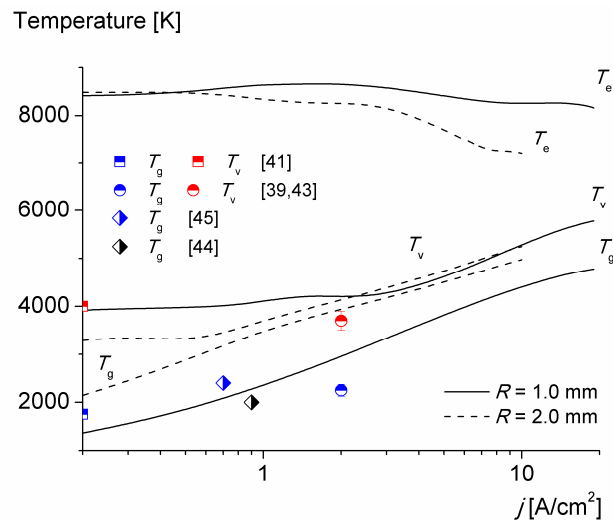


Figure 1. The Electron (T_e), gas (T_g), and vibrational (T_v) temperatures versus the discharge current density.

Figure 2 presents the thermal dissociation for vibrationally excited molecules versus the discharge current density calculated for $R = 1.0$ mm. For comparative purposes, the electron-impact dissociation from all the vibrational levels of $N_2(X^1\Sigma_g^+, v)$ is also shown. As it can be seen, differences with several orders of magnitude between both dissociation rates existed across the whole range of current densities, thus suggesting that the electron-impact dissociation process is not important under the considered low-electric-field conditions. Furthermore, thermal dissociation of vibrationally excited molecules dominated the production of $N(^4S)$ atoms at $j < 1$ A/cm². At higher j values ($T_g > 2000$ K), the production of $N(^4S)$ was mainly controlled by the exchange reaction (R72).

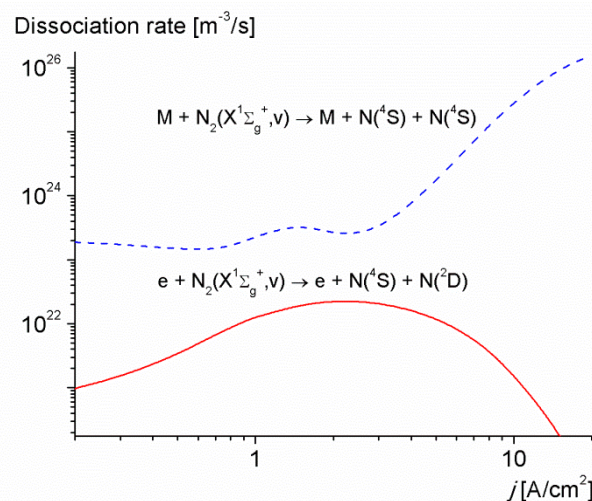


Figure 2. The dissociation rates versus the discharge current density for $R = 1.0$ mm.

The number densities of various neutral particles versus the discharge current density calculated for $R = 1.0$ mm are shown in Figure 3. At low current densities ($j = 0.1$ A/cm²), the concentration of NO was mainly controlled by reactions (R49), (R61), (R62), and (R66). In particular, the production of NO was strongly affected by collisions with $N_2(A^3\Sigma_u^+)$ molecules produced by the electron impact from all the vibrational levels of $N_2(X^1\Sigma_g^+, v)$. Therefore, the densities of NO at low j values were greater than those corresponding to local thermodynamic equilibrium at T_g . At higher current densities ($j > 1$ A/cm²), the densities of NO were governed by reactions with the participation of ground-electronic-state particles reactions (R62) and (R72), balanced by their inverse reactions (R73) and (R61), respectively. These results agreed with the inferences made in [10]. The density of $N_2(A^3\Sigma_u^+)$ molecules was moderately high (5×10^{17} – 8×10^{18} m⁻³) under the conditions considered (although it was at least one order of magnitude lower than that found in atmospheric-pressure nitrogen discharges [47], because $N_2(A^3\Sigma_u^+)$ molecules were efficiently quenched by oxygen), favored by the vibrational nonequilibrium state of the discharge. Note that the rate of population of the $N_2(A^3\Sigma_u^+)$ (and other states) by electron impact became significantly higher, as the degree of vibrational excitation of $N_2(X^1\Sigma_g^+, v)$ molecules increased, which in turn increased the densities of excited $N(^2D)$ and $N(^2P)$ atoms via quenching reactions (R49) and (R50), respectively. The presence of $N_2(A^3\Sigma_u^+)$ also caused a rise in the density of $O(^3P)$ atoms, because O_2 molecules were also dissociated via the quenching reaction (R44). Note also the considerable dissociation degree of nitrogen and oxygen molecules in the discharge. As quoted before, the former was mainly decomposed by thermal dissociation enhanced by vibrational nonequilibrium at $j < 1$ A/cm² and by the exchange reaction (R72) for higher j values, while the latter was mainly decomposed by the exchange reaction (R62) at $j > 1$ A/cm².

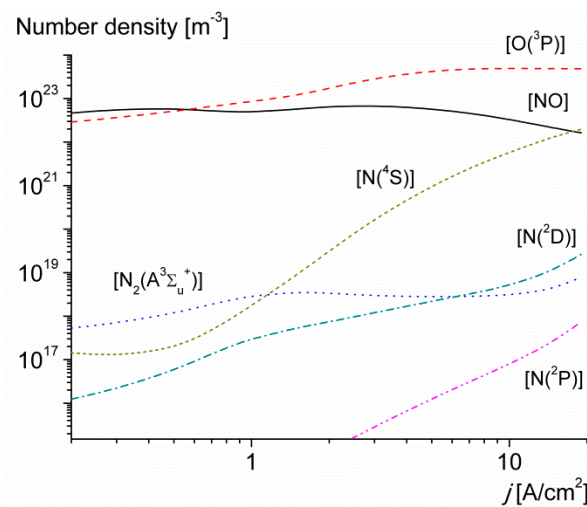
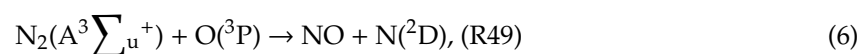
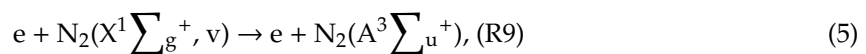


Figure 3. The number densities of some neutral species versus the discharge current density for $R = 1.0$ mm.

Figure 4 depicts various mechanisms for the production and loss of electrons versus the discharge current density calculated for $R = 1.0$ mm. It can be seen that at low current densities ($j < 1$ A/cm²), the production of electrons was dominated by the electron-impact ionization of NO molecules via the reaction (R3) [3,4,8–10]. However, an increase in the current density values (and thus in the gas temperature) progressively changed the ionization kinetics of the discharge at $j > 1$ A/cm² ($T_g > 2500$ K) according to Figure 1, mainly via the following reactions:



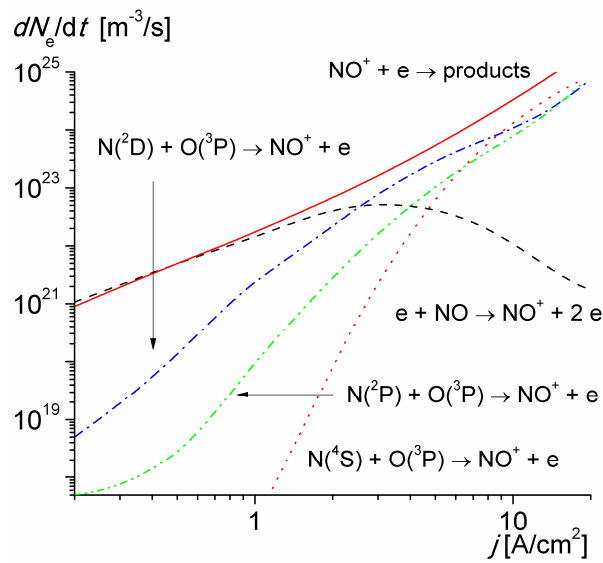
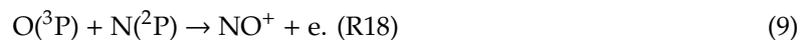
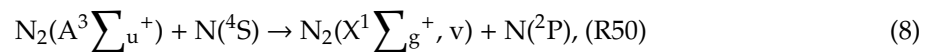


Figure 4. The rates of electron production and loss via various mechanisms versus the discharge current density calculated for $R = 1.0$ mm.

The rate coefficient of reaction (R16) was strongly dependent on T_g and independent of E/N . For higher values of j , the increase in the population of $N(2P)$ also speeded up the ionization due to the growing importance of the reactions:



According to the obtained results, the associative ionization reaction involving $N(2D)$ -excited atoms is the major ionization mechanisms in air at $2500 \text{ K} < T_g < 4500 \text{ K}$. These results are quite different from those found in the literature for similar discharge conditions (e.g., [3,4,10]), which indicate that the electron-impact ionization of NO molecules via reaction (R3) is the major ionization mechanism in air at $1000 \text{ K} < T_g < 4500 \text{ K}$. At $j > 10 \text{ A/cm}^2$ ($T_g > 4500 \text{ K}$), the dominant ionization mechanism became a high-threshold associative ionization reaction in collisions between ground-state atoms indicated by reaction (R13) [10]. However, the reduced electric field still governed the electron density through electron loss, rather than through ionization [10]. The electron-ion-recombination reaction (R23) dominated the loss of electrons across the whole current density range. Since the gas temperature was rather high, there was negligible attachment under the conditions considered.

The calculation and experimental results of the electron number density in plasma versus the discharge current density for $R = 1.0$ mm [36,37] are shown in Figure 5. Good agreement of the calculation results with the experiment results was observed. There was also an increase of one order of magnitude in the calculated electron number density, when the discharge current density was increased by the same amount [7].

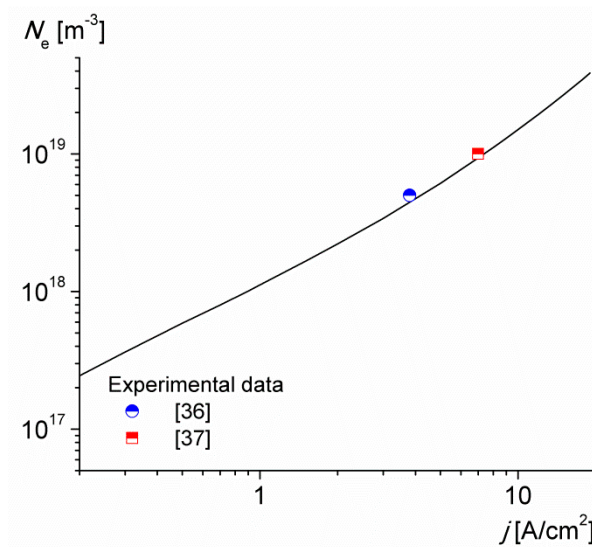


Figure 5. The electron number density in the plasma versus the discharge current density calculated for $R = 1.0$ mm.

Figure 6 presents the reduced electric field ($1 \text{ Td} \equiv 10^{-21} \text{ V m}^2$) versus the discharge current density (i.e., the E/N - j characteristic curve) calculated for $R = 1.0$ mm. Solid and dashed lines are the results of calculations with and without the associative ionization reactions (R16) and (R18), respectively. The characteristic curve given by the solid line follows the changes in the ionization mechanisms shown in Figure 4. It was seen that noticeable differences between both curves exist at current density values of 1–10 A/cm² or when $2500 < T_g < 4500$ K (as shown in Figure 1), i.e., when the associative ionization reaction (R16) becomes the major ionization mechanism in air. It should be noted that the $\text{N}_2(X^1\Sigma_g^+, v)$ vibrationally excited molecules were not directly involved in the reactions of associative ionization but they significantly accelerated the production of $\text{N}_2(A^3\Sigma_u^+)$ molecules in reaction (R9), which in turn increased the densities of excited nitrogen $\text{N}(^2\text{D})$ and $\text{N}(^2\text{P})$ atoms via reactions (R49) and (R50), respectively, participating in the associative ionization reactions (R16) and (R18). Since the electron energy required for the excitation of the $\text{N}_2(A^3\Sigma_u^+)$ state from $\text{N}_2(X^1\Sigma_g^+, v)$ molecules (e.g., 6.2 eV for $v = 0$) was considerably lower than the ionization energy (9.27 eV) of the NO molecules, the reduced electric field began to noticeably fall at $T_g > 2500$ K when the change in the dominant ionization mechanism took place (as shown in Figure 4). That is, long before that the high-threshold associative ionization reaction (R13) began to significantly contribute to the charged particle balance at $T_g > 4000$ K, as was previously reported in the literature (e.g., [3,4,10]).

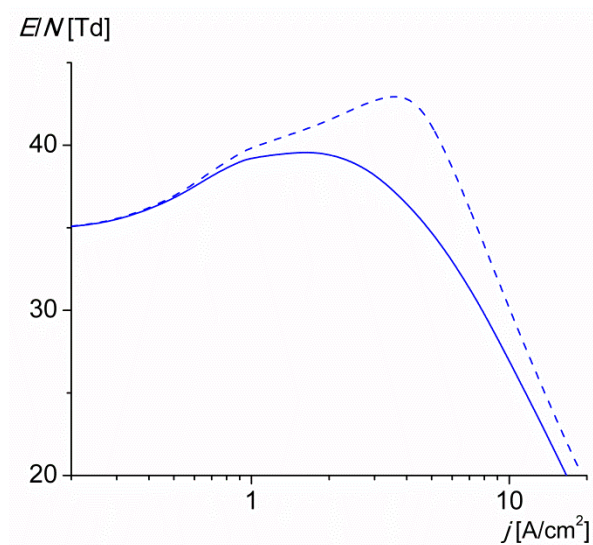


Figure 6. Reduced field versus current density ($E/N-j$) curves calculated for $R = 1.0$ mm with (solid line) and without (dashed line) associative ionization reactions (R16) and (R18).

Figure 7 shows the calculation and experimental results of the reduced electric field versus the discharge current density for $R = 1.0$ mm [3,37,38,42]. It was seen that the calculated $E/N-j$ characteristic showed fairly good agreement with the experimental data, considering the gas temperature variation in various experiments

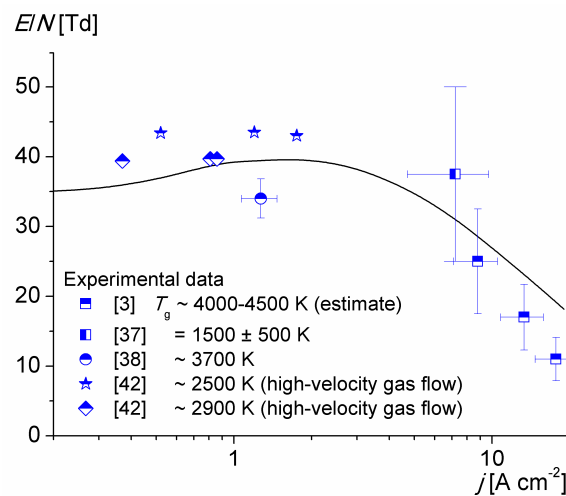


Figure 7. $E/N-j$ characteristic curve calculated for $R = 1.0$ mm.

4. Conclusions

A global model of a stationary glow-type discharge in atmospheric-pressure air was developed. The assumptions of temporal and spatial homogeneity inherent in the global model approach were accurately enough under the conditions considered. Relevant kinetic processes in nitrogen–oxygen ($N_2-20\% O_2$) mixtures at a gas temperature range ($1000 \text{ K} < T_g < 6000 \text{ K}$) were considered. A distinctive feature of the model is that it takes into account associative ionization reactions involving excited atoms, which are not routinely considered in the literature. Thermal dissociation of vibrationally excited nitrogen molecules, as well as electronic excitation from all the vibrational levels of nitrogen molecules was also taken into account. The results of calculations suggested a strong impact of the electronically excited states of reactants on associative ionization reactions in atomic collisions in hot air. It was shown that the near-threshold associative ionization reaction involving $N(^2D)$ atoms progressively replaced

the ionization of NO molecules by electron impact at $T_g > 2500$ K, becoming the main ionization mechanism in air up to 4000–4500 K. As a consequence, the reduced electric field of the discharge began to noticeably fall at $T_g > 2500$ K, when the change in the dominant ionization mechanism took place. The exoergic associative ionization reaction involving $N(^2P)$ atoms also speeded up the ionization at the highest temperature values. The role of processes concerning vibrationally excited nitrogen molecules played a significant role in the air kinetics under the analyzed conditions. The calculated plasma parameters agreed with the available experimental data.

Author Contributions: E.C. and B.M. conceived and developed the numerical model; L.P. contributed to the model kinetic block; all authors wrote, reviewed and approved the final manuscript. All authors have read and agreed to the published version of the manuscript.

Funding: This research was funded by Universidad Tecnológica Nacional (grant numbers: 5418 and 5447) and Agencia Nacional de Promoción Científica y Tecnológica (grant number: PICT 2015 nro. 1553).

Acknowledgments: E.C. thanks CONICET for his doctoral fellowship. L.P. is a member of CONICET.

Conflicts of Interest: The authors declare no conflicts of interest. The funders had no role in the design of the study; in the collection, analyses, or interpretation of data; in the writing of the manuscript, or in the decision to publish the results.

Appendix A

Table A1. List of reactions. T_e and T_g are in Kelvin. Rate coefficients obtained with the help of the BOLSIG+ code were corrected in order to account for gains in electron energy in superelastic collisions [17]. Calculations were performed using rates for reactions (R22) and (R23) taken from [48].

R _j	Reaction	Rate Coefficient (m ³ /s or m ⁶ /s)	Reference
<i>Electron-Impact Processes</i>			
R1	$e + N_2(X) \rightarrow e + e + N_2^+$	$k_1 = f(E/N)$	[49,50]
R2	$e + O_2 \rightarrow e + e + O_2^+$	$k_2 = f(E/N)$	[49,50]
R3	$e + NO \rightarrow e + e + NO^+$	$k_3 = f(E/N)$	[49,50]
R4	$e + O(^3P) \rightarrow e + e + O^+$	$k_4 = f(E/N)$	[49,50]
R5	$e + N_2(X) \rightarrow e + N_2^* (\Delta E = 13 \text{ eV})$ $e + N(^4S) + N(^2D)$	$k_5 = f(E/N)$	[49,50]
R6	$e + O_2 \rightarrow e + O_2^* (\Delta E = 6.0 \text{ eV})$ $e + O(^3P) + O(^3P) + 0.8 \text{ eV}$	$k_6 = f(E/N)$	[49,50]
R7	$e + O_2 \rightarrow e + O_2 (\Delta E = 8.4 \text{ eV})$ $e + O(^3P) + O(^1D) + 1.26 \text{ eV}$	$k_7 = f(E/N)$	[49,50]
R8	$e + O_2 \rightarrow e + O_2 (\Delta E = 9.97 \text{ eV})$ $e + O(^3P) + O(^1S) + 0.6 \text{ eV}$	$k_8 = f(E/N)$	[49,50]
R9	$e + N_2(X) \rightarrow e + N_2(A)$	$k_9 = f(E/N)$	[49,50]
R10	$e + N_2(X) \rightarrow e + N_2(B)$	$k_{10} = f(E/N)$	[49,50]
R11	$e + N_2(X) \rightarrow e + N_2(a')$	$k_{11} = f(E/N)$	[49,50]
R12	$e + N_2(X) \rightarrow e + N_2(C)$	$k_{12} = f(E/N)$	[49,50]
<i>Associative Ionization</i>			
R13	$N(^4S) + O(^3P) \rightarrow NO^+ + e$	$k_{13} = 5 \times 10^{-17} T_g^{-0.5} e^{(-32500/T_g)}$	[51]
R14	$N(^4S) + O(^1S) \rightarrow NO^+ + e$	$k_{14} = (1-3) \times 10^{-17} (T_g/300)^{1/6}$	[18]
R15	$N(^4S) + O(^1D) \rightarrow NO^+ + e$	$k_{15} = 3.1 \times 10^{-25} T_g^{0.5} (9287 + 2T_g) e^{(-9287/T_g)}$	[52]

Table A1. Cont.

R _j	Reaction	Rate Coefficient (m ³ /s or m ⁶ /s)	Reference
R16	N(² D) + O(³ P) → NO ⁺ + e	$k_{16} = 1.3 \times 10^{-24} T_g^{0.5} (4411 + 2T_g) e^{(-4411/T_g)}$	[20,21]
R17	N(² D) + N(² P) → N ₂ ⁺ + e	$k_{17} = 1.9 \times 10^{-21} T_g^{0.98} [1 - e^{(-3129/T_g)}]^{-1}$	[53]
R18	N(² P) + O(³ P) → NO ⁺ + e	$k_{18} = (1-3) \times 10^{-17} (T_g/300)^{1/6}$	[18]
R19	N(² P) + N(² P) → N ₂ ⁺ + e	$k_{19} = 3.2 \times 10^{-21} T_g^{0.98} [1 - e^{(-3129/T_g)}]^{-1}$	[53]
<i>Penning Ionization</i>			
R20	N ₂ (A) + N ₂ (a') → N ₂ ⁺ + N ₂ (X) + e	$k_{20} = 5 \times 10^{-17}$	[54]
R21	N ₂ (a') + N ₂ (a') → N ₂ ⁺ + N ₂ (X) + e	$k_{21} = 2 \times 10^{-16}$	[54]
<i>Dissociative electron–Ion Recombination</i>			
R22	e + NO ⁺ → N(⁴ S) + O(³ P)	$k_{22} = 0.05 \times 1.5 \times 10^{-11} T_e^{-0.65}$ $k_{22} = 0.05 \times 1.1 \times 10^{-8} T_e^{-1.5}$	[55,56] [48]
R23	e + NO ⁺ → N(² D) + O(³ P)	$k_{23} = 0.95 \times 1.5 \times 10^{-11} T_e^{-0.65}$ $k_{23} = 0.95 \times 1.1 \times 10^{-8} T_e^{-1.5}$	[55,56] [48,56]
R24	e + N ₂ ⁺ → N(⁴ S) + N(² D)	$k_{24} = 0.46 \times 2.0 \times 10^{-13} (300/T_e)^{0.5}$	[22,57]
R25	e + N ₂ ⁺ → N(⁴ S) + N(² P)	$k_{25} = 0.08 \times 2.0 \times 10^{-13} (300/T_e)^{0.5}$	[22,57]
R26	e + N ₂ ⁺ → N(² D) + N(² D)	$k_{26} = 0.46 \times 2.0 \times 10^{-13} (300/T_e)^{0.5}$	[22,57]
R27	e + O ₂ ⁺ → O(³ P) + O(³ P)	$k_{27} = 0.32 \times 2.0 \times 10^{-13} (300/T_e)$	[22,57]
R28	e + O ₂ ⁺ → O(³ P) + O(¹ D)	$k_{28} = 0.43 \times 2.0 \times 10^{-13} (300/T_e)$	[22,57]
R29	e + O ₂ ⁺ → O(¹ D) + O(¹ D)	$k_{29} = 0.20 \times 2.0 \times 10^{-13} (300/T_e)$	[22,57]
R30	e + O ₂ ⁺ → O(¹ D) + O(¹ S)	$k_{30} = 0.05 \times 2.0 \times 10^{-13} (300/T_e)$	[22,57]
<i>Three Body Electron–Ion Recombination</i>			
R31	e + e + O ⁺ → e + O(³ P)	$k_{31} = 1.0 \times 10^{-31} (300/T_e)^{4.5}$	[22]
<i>Thermal Dissociation/Three-Body Recombination</i>			
R32	N ₂ (X) + M → N(⁴ S) + N(⁴ S) + M M = N ₂ (X), O ₂ , and NO	$k_{32} = 5 \times 10^{-14} e^{(-113200/T_g)}$ $[1 - e^{(-3354/T_g)}]$	[10]
R33	N ₂ (X) + M → N(⁴ S) + N(⁴ S) + M M = N(⁴ S) and O(³ P)	$k_{33} = 1.1 \times 10^{-13} e^{(-113200/T_g)}$ $[1 - e^{(-3354/T_g)}]$	[10]
R34	N(⁴ S) + N(⁴ S) + M → N ₂ (X) + M M = N ₂ (X), O ₂ , NO, O(³ P), N(⁴ S)	$k_{34} = 8.27 \times 10^{-46} e^{(500/T_g)}$	[10]
R35	O ₂ (X) + M → O(³ P) + O(³ P) + M M = O ₂	$k_{35} = 3.7 \times 10^{-14} e^{(-59380/T_g)}$ $[1 - e^{(-2240/T_g)}]$	[10]
R36	O ₂ (X) + M → O(³ P) + O(³ P) + M M = O(³ P)	$k_{36} = 1.3 \times 10^{-13} e^{(-59380/T_g)}$ $[1 - e^{(-2240/T_g)}]$	[10]
R37	O ₂ (X) + M → O(³ P) + O(³ P) + M M = N ₂ (X), N(⁴ S), and NO	$k_{37} = 9.3 \times 10^{-15} e^{(-59380/T_g)}$ $[1 - e^{(-2240/T_g)}]$	[10]
R38	O(³ P) + O(³ P) + M → O ₂ (X) + M M = N ₂ (X)	$k_{38} = 2.76 \times 10^{-46} e^{(720/T_g)}$	[10]
R39	O(³ P) + O(³ P) + M → O ₂ (X) + M M = O ₂	$k_{39} = 2.45 \times 10^{-43} T_g^{-0.63}$	[10]

Table A1. Cont.

R _j	Reaction	Rate Coefficient (m ³ /s or m ⁶ /s)	Reference
R40	O(³ P) + O(³ P) + M → O ₂ (X) + M M = O(³ P)	$k_{40} = 8.8 \times 10^{-43} T_g^{-0.63}$	[10]
R41	NO + M → N(⁴ S) + O(³ P) + M M = N ₂ (X) and O ₂	$k_{41} = 8.7 \times 10^{-15} e^{(-76000/Tg)}$	[10]
R42	NO + M → N(⁴ S) + O(³ P) + M M = O(³ P) and NO	$k_{42} = 1.7 \times 10^{-13} e^{(-76000/Tg)}$	[10]
R43	N(⁴ S) + O(³ P) + M → NO(X) + M M = N ₂ (X), O ₂ , NO, and O(³ P)	$k_{43} = 1.76 \times 10^{-43} T_g^{-0.5}$	[10]
<i>Chemical Reactions</i>			
R44	N ₂ (A) + O ₂ → N ₂ (X) + 2 O(³ P) + 1.1 eV	$k_{44} = 1.7 \times 10^{-18}$	[58]
R45	N ₂ (A) + O ₂ → N ₂ (X) + O ₂ (b)	$k_{45} = 7.5 \times 10^{-19}$	[58]
R46	N ₂ (A) + N ₂ (A) → N ₂ (X) + N ₂ (B)	$k_{46} = 7.7 \times 10^{-17}$	[59]
R47	N ₂ (A) + N ₂ (A) → N ₂ (X) + N ₂ (C)	$k_{47} = 1.6 \times 10^{-16}$	[59]
R48	N ₂ (A) + O(³ P) → N ₂ (X) + O(¹ S)	$k_{48} = 2.1 \times 10^{-17}$	[22]
R49	N ₂ (A) + O(³ P) → NO + N(² D)	$k_{49} = 7.0 \times 10^{-18}$	[22]
R50	N ₂ (A) + N(⁴ S) → N ₂ (X) + N(² P)	$k_{50} = 5.0 \times 10^{-17}$	[60]
R51	N ₂ (A) + NO → N ₂ (X) + NO	$k_{51} = 6.4 \times 10^{-17}$	[58]
R52	N ₂ (B) + O ₂ → N ₂ (X) + 2 O(³ P)	$k_{52} = 3.0 \times 10^{-16}$	[22]
R53	N ₂ (B) + N ₂ (X) → N ₂ (X) + N ₂ (A)	$k_{53} = 1.0 \times 10^{-17}$	[60]
R54	N ₂ (a') + O ₂ → N ₂ (X) + O(³ P) + O(¹ D) + 1.4 eV	$k_{54} = 2.8 \times 10^{-17}$	[22]
R55	N ₂ (a') + N ₂ (X) → N ₂ (X) + N ₂ (B)	$k_{55} = 2.0 \times 10^{-19}$	[22]
R56	N ₂ (a') + O(³ P) → NO + N(² D)	$k_{56} = 3.0 \times 10^{-16}$	[61]
R57	N ₂ (a') + NO → N(⁴ S) + O(³ P) + N ₂ (X)	$k_{57} = 3.6 \times 10^{-16}$	[62]
R58	N ₂ (C) + O ₂ → N ₂ (X) + 2O(³ P)	$k_{58} = 2.5 \times 10^{-16}$	[63]
R59	N ₂ (C) + N ₂ (X) → N ₂ (X) + N ₂ (B)	$k_{59} = 1.0 \times 10^{-17}$	[63]
R60	N ₂ (C) → N ₂ (B) + <i>hν</i>	$k_{60} = 2.4 \times 10^7 \text{ s}^{-1}$	[22]
R61	N(⁴ S) + NO → O(³ P) + N ₂ (X)	$k_{61} = 1.0 \times 10^{-18} T_g^{0.5}$	[22]
R62	N(⁴ S) + O ₂ → O(³ P) + NO	$k_{62} = 1.1 \times 10^{-20} T_g e^{(-3150/Tg)}$	[22]
R63	N(² D) + N ₂ (X) → N(⁴ S) + N ₂ (X)	$k_{63} = 1.7 \times 10^{-20}$	[58]
R64	N(² D) + O(³ P) → N(⁴ S) + O(³ P)	$k_{64} = 1.4 \times 10^{-18}$	[58]
R65	N(² D) + O ₂ → NO + O(³ P)	$k_{65} = 2.4 \times 10^{-18} e^{(-185/Tg)}$	[58]
R66	N(² D) + O ₂ → NO + O(¹ D)	$k_{66} = 7.3 \times 10^{-18} e^{(-185/Tg)}$	[58]
R67	N(² D) + NO → N ₂ (X) + O(¹ S)	$k_{67} = 6.0 \times 10^{-17}$	[58]
R68	N(² P) + N(⁴ S) → N(² D) + N(⁴ S)	$k_{68} = 1.8 \times 10^{-18}$	[22]
R69	N(² P) + O(³ P) → N(² D) + O(³ P)	$k_{69} = 1.0 \times 10^{-18}$	[60]
R70	N(² P) + O ₂ → NO + O(³ P)	$k_{70} = 2.5 \times 10^{-18}$	[58]
R71	N(² P) + NO → N ₂ (X) + O(³ P)	$k_{71} = 2.9 \times 10^{-17}$	[58]

Table A1. Cont.

R _j	Reaction	Rate Coefficient (m ³ /s or m ⁶ /s)	Reference
R72	O(³ P) + N ₂ (X) → N(⁴ S) + NO	$k_{72} = 1.3 \times 10^{-16} e^{(-3800/T_g)}$	[10]
R73	O(³ P) + NO → N(⁴ S) + O ₂	$k_{73} = 2.5 \times 10^{-21} T_g e^{(-19500/T_g)}$	[10]
R74	O(¹ D) + O(³ P) → O(³ P) + O(³ P)	$k_{74} = 8.0 \times 10^{-18}$	[22]
R75	O(¹ D) + O ₂ → O(³ P) + O ₂ (b)	$k_{75} = 3.2 \times 10^{-17} e^{(67/T_g)}$	[22]
R76	O(¹ D) + N ₂ (X) → O(³ P) + N ₂ (X) + 1.4 eV	$k_{76} = 1.8 \times 10^{-17} e^{(107/T_g)}$	[22]
R77	O(¹ S) + O(³ P) → O(¹ D) + O(³ P)	$k_{77} = 5.0 \times 10^{-17} e^{(-301/T_g)}$	[22]
R78	O(¹ S) + O ₂ → O ₂ + O(³ P)	$k_{78} = 3.0 \times 10^{-18} e^{(-850/T_g)}$	[22]
R79	O(¹ S) + O ₂ → O ₂ + O(¹ D)	$k_{79} = 1.3 \times 10^{-18} e^{(-850/T_g)}$	[22]
R80	O(¹ S) + N(⁴ S) → O(³ P) + N(² P)	$k_{80} = 1.0 \times 10^{-18}$	[60]
R81	O(¹ S) + NO → O(³ P) + NO	$k_{81} = 1.8 \times 10^{-16}$	[22]
R82	O(¹ S) + NO → O(¹ D) + NO	$k_{82} = 3.2 \times 10^{-16}$	[22]
<i>Electron Attachment and Detachment</i>			
R83	e + O ₂ + O ₂ → O ₂ ⁻ + O ₂	$k_{83} = 1.4 \times 10^{-41} (300/T_e) e^{(-660/T_g)} e^{[700 (T_e - T_g)/(T_e T_g)]}$	[22]
R84	e + O ₂ → O ⁻ + O(³ P)	$k_{84} = f(E/N)$	[49,50]
R85	O ₂ ⁻ + O ₂ → O ₂ + O ₂ + e	$k_{85} = 2.7 \times 10^{-16} (T_g/300)^{0.5} e^{(-5590/T_g)}$	[22]
R86	O ₂ ⁻ + O(³ P) → O ₃ + e	$k_{86} = 1.5 \times 10^{-16}$	[22]
R87	O ⁻ + N ₂ (X) → N ₂ O + e	$k_{87} = 9.0 \times 10^{-19}$	[22]
R88	O ⁻ + O(³ P) → O ₂ + e	$k_{88} = 5.0 \times 10^{-16}$	[22]
R89	O ⁻ + NO → NO ₂ + e	$k_{89} = 2.6 \times 10^{-16}$	[22]
R90	O ₃ ⁻ + O(³ P) → O ₂ + O ₂ + e	$k_{90} = 3.0 \times 10^{-16}$	[22]
<i>Ion Conversion</i>			
R91	O ⁻ + O ₂ (X) + M → O ₃ ⁻ + M M = N ₂ (X), O ₂	$k_{91} = 1.1 \times 10^{-42} (300/T_g)$	[22]
R92	O ⁺ + N ₂ (X) → NO ⁺ + N(⁴ S)	$k_{92} = (1.5 - 2.0 \times 10^{-3} T_g + 9.56 \times 10^{-7} T_g^2) \times 10^{-18}$	[60]
R93	N ₂ ⁺ + O ₂ (X) → N ₂ (X) + O ₂ ⁺	$k_{93} = 6 \times 10^{-17} (300/T_g)^{0.5}$	[22]
R94	N ₂ ⁺ + O(³ P) → N ₂ (X) + O ⁺	$k_{94} = 1.0 \times 10^{-17} (300/T_g)^{0.2}$	[22]
R95	N ₂ ⁺ + O(³ P) → NO ⁺ + N(⁴ S)	$k_{95} = 0.95 \times 1.3 \times 10^{-16} (300/T_g)^{0.5}$	[22,64]
R96	N ₂ ⁺ + O(³ P) → NO ⁺ + N(² D)	$k_{96} = 0.05 \times 1.3 \times 10^{-16} (300/T_g)^{0.5}$	[22,64]
R97	O ₂ ⁺ + NO → NO ⁺ + O ₂	$k_{97} = 6.3 \times 10^{-16}$	[60]
<i>Ion-Ion Recombination</i>			
R98	X ⁻ + Y ⁺ → X + Y X ⁻ = O ⁻ , O ₂ ⁻ , and O ₃ ⁻ Y ⁺ = N ₂ ⁺ , O ₂ ⁺ , NO ⁺ , and O ⁺	$k_{98} = 2.0 \times 10^{-13} (300/T_g)^{0.5}$	[22]

References

1. Naidis, G.V. Simulation of streamer-to-spark transition in short non-uniform air gaps. *J. Phys. D Appl. Phys.* **1999**, *32*, 2649–2654. [[CrossRef](#)]
2. Naidis, G.V. Dynamics of streamer breakdown of short non-uniform air gaps. *J. Phys. D Appl. Phys.* **2005**, *38*, 3889–3893. [[CrossRef](#)]
3. Prevosto, L.; Kelly, H.; Mancinelli, B.; Chamorro, J.C.; Cejas, E. On the physical processes ruling an atmospheric pressure air glow discharge operating in an intermediate current regime. *Phys. Plasmas* **2015**, *22*, 023504. [[CrossRef](#)]
4. Benilov, M.S.; Naidis, G.V. Modelling of low-current discharges in atmospheric-pressure air taking account of non-equilibrium effects. *J. Phys. D Appl. Phys.* **2003**, *36*, 1834–1841. [[CrossRef](#)]
5. Naidis, G.V. Simulation of convection-stabilized low-current glow and arc discharges in atmospheric-pressure air. *Plasma Sources Sci. Technol.* **2007**, *16*, 297–303. [[CrossRef](#)]
6. Xaubet, M.; Giuliani, L.; Grondona, D.; Minotti, F. Experimental and theoretical study of an atmospheric air plasma-jet. *Phys. Plasmas* **2017**, *24*, 013502. [[CrossRef](#)]
7. Laux, C.O.; Yu, L.; Packan, D.M.; Gessman, R.J.; Pierrot, L.; Kruger, C.H.; Zare, R.N. Ionization Mechanisms in Two-Temperature Air Plasmas. In Proceedings of the 30th Plasmadynamic and Lasers Conference, Norfolk, VA, USA, 28 June–1 July 1999.
8. Benilov, M.S.; Naidis, G.V. Modelling of discharges in a flow of preheated air. *Plasma Sources Sci. Technol.* **2005**, *16*, 129–133. [[CrossRef](#)]
9. Popov, N.A. Simulations of a longitudinal glow discharge in a hot air flow at atmospheric pressure. *Plasma Phys. Rep.* **2006**, *32*, 237–245. [[CrossRef](#)]
10. Aleksandrov, N.L.; Bazelyan, E.M.; Kochetov, I.V.; Dyatko, N.A. The ionization kinetics and electric field in the leader channel in long air gaps. *J. Phys. D Appl. Phys.* **1997**, *30*, 1616–1624. [[CrossRef](#)]
11. Popov, N.A. Formation and Development of a Leader Channel in Air. *Plasma Phys. Rep.* **2003**, *29*, 695–708. [[CrossRef](#)]
12. da Silva, C.L.; Pasko, V.P. Dynamics of streamer-to-leader transition at reduced air densities and its implications for propagation of lightning leaders and gigantic jets. *J. Geophys. Res.* **2013**, *118*, 13561–13590. [[CrossRef](#)]
13. Aleksandrov, N.L.; Bazelyan, E.M. Ionization processes in spark discharge plasmas. *Plasma Sources Sci. Technol.* **1999**, *8*, 285–294. [[CrossRef](#)]
14. Aleksandrov, N.L.; Bazelyan, E.M.J. The mechanism of re-breakdown within a post-arc channel in long non-uniform air gaps. *Phys. D Appl. Phys.* **1998**, *31*, 1343–1351. [[CrossRef](#)]
15. Aleksandrov, N.L.; Bazelyan, E.M.; Konchakov, A.M. Plasma Parameters in the Channel of a Long Leader in Air. *Plasma Phys. Rep.* **2001**, *27*, 875–885. [[CrossRef](#)]
16. Mankelevich, Y.A.; Pal, A.F.; Popov, N.A.; Rakhimova, T.V.; Filippov, A.V. Current Dynamics and Mechanisms for the Instability of a Non-Self-Sustained Glow Discharge in Nitrogen. *Plasma Phys. Rep.* **2001**, *27*, 979–989. [[CrossRef](#)]
17. Cejas, E.; Mancinelli, B.R.; Prevosto, L. Glow Discharge in a High-Velocity Air Flow: The Role of the Associative Ionization Reactions Involving Excited Atoms. *Materials* **2019**, *12*, 2524. [[CrossRef](#)] [[PubMed](#)]
18. Chernyi, G.G.; Losev, S.A.; Macheret, S.O.; Potapkin, B.V. *Physical and Chemical Processes in Gas Dynamics: Cross Sections and Rate Constants Vol. 1*; AIAA: Reston, VA, USA, 2002; pp. 237–297.
19. Piper, L.G. The reactions of $N(^2P)$ with O_2 and O . *J. Chem. Phys.* **1993**, *98*, 8560–8564. [[CrossRef](#)]
20. Golubkov, G.V.; Ozerov, G.K. The Near-Threshold Associative Ionization $N(^2D) + O(^3P) \rightarrow NO(X^1\Sigma^+) + e^-$ Reaction. *Doklady Phys.* **2014**, *59*, 122–125. [[CrossRef](#)]
21. Ringer, G.; Gentry, W.R. A merged molecular beam study of the endoergic associative ionization reaction $N(^2D) + O(^3P) \rightarrow NO^+ + e^-$. *J. Chem. Phys.* **1979**, *71*, 1902–1909. [[CrossRef](#)]
22. Kossyi, I.A.; Kostinsky, A.Y.; Matveyev, A.A.; Silakov, V.P. Kinetic scheme of the non-equilibrium discharge in nitrogen-oxygen mixtures. *Plasma Sources Sci. Technol.* **1992**, *1*, 207–220. [[CrossRef](#)]
23. Capitelli, M.; Ferreira, C.M.; Gordiets, B.F.; Osipov, A.I. *Plasma Kinetics in Atmospheric Gases*; Springer: New York, NY, USA, 2000; pp. 66–154.

24. Hurlbatt, A.; Gibson, A.R.; Schroter, S.; Bredin, J.; Foote, A.P.S.; Grondein, P.; O'Connell, D.; Gans, T. Concepts, Capabilities, and Limitations of Global Models: A Review. *Plasma Process. Polym.* **2017**, *14*, 1600138. [[CrossRef](#)]
25. Boeuf, J.P.; Kunhardt, E.E. Energy balance in a nonequilibrium weakly ionized nitrogen discharge. *J. Appl. Phys.* **1986**, *60*, 915–923. [[CrossRef](#)]
26. Breshears, W.D.; Bird, P.F. Effect of Oxygen Atoms on the Vibrational Relaxation of Nitrogen. *J. Chem. Phys.* **1968**, *48*, 4768–4773. [[CrossRef](#)]
27. Eckstrom, D.J. Vibrational relaxation of shockheated N₂ by atomic oxygen using the ir tracer method. *J. Chem. Phys.* **1973**, *59*, 2787–2795. [[CrossRef](#)]
28. McNeal, R.J.; Whitson, M.E.; Cooke, G.R. Temperature Dependence of the Quenching of Vibrationally Excited Nitrogen by Atomic Oxygen. *J. Geophys. Res.* **1974**, *79*, 1527–1531. [[CrossRef](#)]
29. Popov, N.A. Investigation of the Mechanism for Rapid Heating of Nitrogen and Air in Gas Discharges. *Plasma Phys. Rep.* **2001**, *27*, 886–896. [[CrossRef](#)]
30. Pintassilgo, C.D.; Guerra, V. On the different regimes of gas heating in air plasmas. *Plasma Sources Sci. Technol.* **2015**, *24*, 055009. [[CrossRef](#)]
31. D'Angola, A.; Colonna, G.; Bonomo, A.; Bruno, D.; Laricchiuta, A.; Capitelli, M. A phenomenological approach for the transport properties of air plasmas. *Eur. Phys. J. D* **2012**, *66*, 205. [[CrossRef](#)]
32. Bruggeman, P.J.; Iza, F.; Brandenburg, R. Foundations of atmospheric pressure non-equilibrium plasmas. *Plasma Sources Sci. Technol.* **2017**, *26*, 123002. [[CrossRef](#)]
33. Adamovich, I.; Baalrud, S.D.; Bogaerts, A.; Bruggeman, P.J.; Cappelli, M.; Colombo, V.; Czarnetzki, U.; Ebert, U.; Eden, J.G.; Favia, P.; et al. The 2017 Plasma Roadmap: Low temperature plasma science and technology. *J. Phys. D Appl. Phys.* **2017**, *50*, 323001. [[CrossRef](#)]
34. Schoenbach, K.H.; Becker, K. 20 years of microplasma research: A status report. *Eur. Phys. J. D* **2016**, *70*, 29. [[CrossRef](#)]
35. André, P.; Barinov, Y.A.; Faure, G.; Shkol'nik, S.M. Characteristics of discharge with liquid nonmetallic cathode burning in air flow. *J. Phys. D Appl. Phys.* **2018**, *51*, 445202. [[CrossRef](#)]
36. Stark, R.H.; Schoenbach, K.H. Direct current glow discharges in atmospheric air. *Appl. Phys. Lett.* **1999**, *74*, 3770–3772. [[CrossRef](#)]
37. Leipold, F.; Stark, R.H.; El-Habachi, A.; Schoenbach, K.H. Electron density measurements in an atmospheric pressure air plasma by means of infrared heterodyne interferometry. *J. Phys. D Appl. Phys.* **2000**, *33*, 2268–2273. [[CrossRef](#)]
38. Machala, Z.; Laux, C.O.; Kruger, C.H.; Candler, G.V. Atmospheric Air and Nitrogen DC Glow Discharges with Thermionic Cathodes and Swirl Flow. In Proceedings of the 42nd AIAA Aerospace Sciences Meeting and Exhibit, Reno, NV, USA, 5–8 January 2004.
39. Machala, Z.; Janda, M.; Hensel, K.; Jedlovský, I.; Leštinská, L.; Foltin, V.; Martišoviš, V.; Morvová, M. Emission spectroscopy of atmospheric pressure plasmas for bio-medical and environmental applications. *J. Mol. Spectrosc.* **2007**, *243*, 194–201. [[CrossRef](#)]
40. Lu, X.P.; Leipold, F.; Laroussi, M. Optical and electrical diagnostics of a non-equilibrium air plasma. *J. Phys. D Appl. Phys.* **2003**, *36*, 2662. [[CrossRef](#)]
41. Andre, P.; Barinov, Y.; Faure, G.; Kaplan, V.; Lefort, A.; Shkol'nik, S.; Vacher, D. Experimental study of discharge with liquid non-metallic (tap-water) electrodes in air at atmospheric pressure. *J. Phys. D: Appl. Phys.* **2001**, *34*, 3456. [[CrossRef](#)]
42. Yu, L.; Laux, C.O.; Packan, D.M.; Kruger, C.H.J. Direct-current glow discharges in atmospheric pressure air plasmas. *Appl. Phys.* **2002**, *91*, 2678–2686. [[CrossRef](#)]
43. Machala, Z.; Marode, E.; Laux, C.O.; Kruger, C.H.J. DC Glow Discharges in Atmospheric Pressure Air. *Adv. Oxid. Technol.* **2004**, *7*, 133–137. [[CrossRef](#)]
44. Duten, X.; Packan, D.; Yu, L.; Laux, C.O.; Kruger, C.H. DC and Pulsed Glow Discharges in Atmospheric Pressure Air and Nitrogen. *IEEE Trans. Plasma Sci.* **2002**, *30*, 178–179. [[CrossRef](#)]
45. Stepianiuk, V.P.; Ioppolo, T.; Ötügen, M.V.; Sheverev, V.A. Measurement of gas temperature and convection velocity profiles in a dc atmospheric glow discharge. *J. Appl. Phys.* **2007**, *102*, 123302. [[CrossRef](#)]
46. Akishev, Y.; Grushin, M.; Karalnik, V.; Petryakov, A.; Trushkin, N. On basic processes sustaining constricted glow discharge in longitudinal N₂ flow at atmospheric pressure. *J. Phys. D Appl. Phys.* **2010**, *43*, 215202. [[CrossRef](#)]

47. Prevosto, L.; Kelly, H.; Mancinelli, B. Modelling of an Atmospheric Pressure Nitrogen Glow Discharge Operating in High-Gas Temperature Regimes. *Plasma Chem. Plasma Process.* **2016**, *36*, 973–992. [CrossRef]
48. Kang, S.W.; Jones, W.L.; Dunn, M.G. Theoretical and Measured Electron-Density Distributions at High Altitudes. *AIAA J.* **1973**, *11*, 141–149. [CrossRef]
49. Hagelaar, G.J.M.; Pitchford, L.C. Solving the Boltzmann equation to obtain electron transport coefficients and rate coefficients for fluid models. *Plasma Sources Sci. Technol.* **2005**, *14*, 722–733, Freeware Code BOLSIG + Version 07/2015. Available online: <http://www.bolsig.laplace.univ-tlse.fr> (accessed on 14 November 2015). [CrossRef]
50. SIGLO. Database. Available online: <http://www.lxcat.laplace.univ-tlse.fr> (accessed on 4 June 2013).
51. Lin, S.C.; Teare, J.D. Rate of Ionization behind Shock Waves in Air. II. Theoretical Interpretations. *Phys. Fluids* **1963**, *6*, 355–375. [CrossRef]
52. Le Padellec, A. Partial near Threshold Cross Sections for the Associative Ionization to Form CO+, NO+ and O2+. *Phys. Scr.* **2005**, *71*, 621–626. [CrossRef]
53. Matveyev, A.A.; Silakov, V.P. Theoretical study of the role of ultraviolet radiation of the non-equilibrium plasma in the dynamics of the microwave discharge in molecular nitrogen. *Plasma Sources Sci. Technol.* **1999**, *8*, 162–178. [CrossRef]
54. Brunet, H.; Roca Serra, J. Model for a glow discharge in flowing nitrogen. *J. Appl. Phys.* **1985**, *57*, 1574–1581. [CrossRef]
55. Park, C. A Review of Reaction Rates in High Temperature Air. In Proceedings of the 24th Thermophysics Conference, Buffalo, NY, USA, 12–14 June 1989.
56. Hellberg, F.; Rosén, S.; Thomas, R.; Neau, A.; Larsson, M.; Petrigiani, P.; van der Zande, W.J. Dissociative recombination of NO+: Dynamics of the X1 Σ^+ and a3 Σ^+ electronic states. *J. Chem. Phys.* **2003**, *118*, 6250–6259. [CrossRef]
57. Florescu, A.I.; Mitchell, J.B.A. Dissociative recombination. *Phys. Rep.* **2006**, *430*, 277–374.
58. Herron, J.T. Evaluated Chemical Kinetics Data for Reactions of N(²D), N(²P), and N₂(A³ Σ_u^+) in the Gas Phase. *J. Phys. Chem. Ref. Data* **1999**, *28*, 1453–1483. [CrossRef]
59. Piper, L.G. Statetostate N₂(A³ Σ_u^+) energy pooling reactions. II. The formation and quenching of N₂(B³ Π_g , v'=1–12). *J. Chem. Phys.* **1988**, *88*, 6911–6921. [CrossRef]
60. Gordiets, B.F.; Ferreira, C.M.; Guerra, V.L.; Loureiro, J.M.A.H.; Nahorny, J.; Pagnon, D.; Touzeau, M.; Vialle, M. Kinetic Model of a Low-Pressure N₂-O₂ Flowing Glow Discharge. *IEEE Trans. Plasma Sci.* **1995**, *23*, 750–768. [CrossRef]
61. Shkurenkov, I.; Burnette, D.; Lempert, W.R.; Adamovich, I.V. Kinetics of excited states and radicals in a nanosecond pulse discharge and afterglow in nitrogen and air. *Plasma Sources Sci. Technol.* **2014**, *23*, 065003. [CrossRef]
62. Piper, L.G. Quenching rate coefficients for N₂(a'¹ Σ_u^-). *J. Chem. Phys.* **1987**, *87*, 1625–1629. [CrossRef]
63. Pancheshnyi, S.V.; Starikovskaia, S.M.; Starikovskii, A.Y. Collisional deactivation of N₂(C³ Π_u , v=0,1,2,3) states by N₂, O₂, H₂ and H₂O molecules. *Chem. Phys.* **2000**, *262*, 349–357. [CrossRef]
64. Siskind, D.E.; Barth, D.A.; Cleary, D.D. The Possible Effect of Solar Soft X Rays on Thermospheric Nitric Oxide. *J. Geophys. Res.* **1990**, *95*, 4311–4317. [CrossRef]

